POLISH MARITIME RESEARCH 4 (128) 2025 Vol. 32; pp. 87-96
10.2478/pomr-2025-0052

Multi-Symptom Diagnostic Investigation of the Working Process of a Marine Diesel Engine: Case Study

Part 2
Simulation Diagnostics

Zbigniew Korczewski [1,*]
Roman Varbanets [2]
Dmytro Minchev [2]
Jacek Rudnicki [1]
[1] Gdansk University of Technology, Gdansk, Poland
[2] Odesa National Maritime University, Odesa, Ukraine

* Corresponding author: *zbikorcz@pg.edu.pl (Zbigniew Korczewski)*

ABSTRACT

This second part of our manuscript deals with the diagnostic capabilities of the Blitz-PRO utility computer program. These capabilities form the basis of the Weichai WP4 engine's digital twin, in terms of multi-symptom identification of selected states of the engine's fed system and valve train system. These states include the use of non-standard fuel, the wear of precision pairs of the high-pressure fuel pump, and mismatched camshaft positioning during engine assembly after maintenance. The basic assumptions of the mathematical model of the diesel engine used in Blitz-PRO are outlined here, and numerical experiments are conducted on the model to simulate the behaviour of the Weichai WP4 engine after the introduction of the considered states. Based on the results of numerical simulations of the working process, a relational model is proposed, which forms the basis for diagnostic reasoning. A comparative analysis of the changes in the diagnostic parameters of the relational model and the resulting syndromes enables early detection of similar states of fuel-fed systems for similar engine types.

Keywords: marine diesel engine, working process, multi-symptom diagnostics, measurement and numerical experiments

INTRODUCTION

The basis for contemporary diagnostics of marine diesel engines is mathematical modelling of the operational process, which is used to develop a virtual reality system called a "digital twin" [1]. This enables computer simulations of the influence of the numerous factors determining the desired values of the engine's thermodynamic cycle parameters, with the aim of achieving maximum thermal efficiency and minimal emissions of harmful (including toxic) components in the exhaust gases. For example, the influence of the fuel injection process, the quality of its atomisation, evaporation, and mixing with air in the combustion chamber can be analysed in terms of the intensity of heat release in the combustion process and the in-cylinder pressure [2-5]. This enables optimisation of the parameters and characteristics of the abovementioned factors, provided that the mathematical model has previously been positively verified through laboratory and engine tests [6-8]. This is a particularly complex issue, because modern marine engines are characterised by significant technological advancements, which introduce significant peculiarities to the modelling of the energy and physicochemical processes. One example involves high-pressure storage fuel injection systems ('common rail' systems) with solenoid- or piezoelectrically controlled injectors, which enable multiple fuel injections with precise control over the number, speed, and duration of injections, regardless of the engine speed or load, as well as sequentially engaged turbochargers with adjusTable geometry [9]. In such cases, conventional single or even double Wiebe functions are no longer suiTable for modelling the fuel combustion rate in contemporary marine diesel engines. Hence, much more complex empirical functions are required to represent the impact of these design parameters on the performance, efficiency and exhaust composition of the engine [10].

Another problem that may be encountered is limited access to detailed technical data on the diagnosed engine, especially in terms of the structural drawings that are necessary for digital dimensioning of the structural parameters, which are then entered into the mathematical model (e.g. by means of the AutoCAD computer application). It should also be mentioned that other input parameters can be introduced into the mathematical model arbitrarily or based on known empirical relationships, which crucially determines the adequacy of the mathematical model.

A further problem is the possibility of verification using a real object (i.e. a full-sized marine engine), which is usually equipped only with a standard measuring system, without the possibility of direct, continuous, and sufficiently in-depth observation of the working process [11-13].

In such a situation, in accordance with the theory of process mathematical modelling and methods of planning experimental research (as described in [14-16]), there are two possible courses of action:

(i) A deductive (deterministic) approach: Starting from the theoretical foundations of the modelled process and based on certain simplifying assumptions, mathematical equations are formulated that establish relationships between the input and output signals of the engine's working spaces (known as 'balance equations'), using the fundamental laws of physics and chemistry (e.g. conservation laws). The mathematical model of the working process developed in this way should be verified by comparing the results of numerical simulations with those of experimental studies of the same processes for a real object, using the same inputs (forcings). This process determines the adequacy of the model, taking into account the measurement uncertainty and the individual design and process characteristics of each real object (production uniqueness). A key issue, however, involves determining the level of detail for the developed mathematical model, since over-enrichment or over-simplification of the model's structure can erase (falsify) the actual picture of the engine performance. An overly detailed model, enriched with details and elements that contribute little to the intended purpose of the simulation, significantly complicates the calculation procedures, and consequently the assessment of the adequacy of the obtained simulation results and their further interpretation. Conversely, an overly simplified model is often unreliable.

(ii) An inductive (probabilistic) approach: Through carefully scheduled experiments, engine tests are first conducted on a real object. The courses of the output signals are determined for specific (appropriately planned) alterations to the input signals. Based on a regression analysis of both types of signal, the mathematical relationships between them are established (as a function of the research object, in this case a heat release rate) and verified in accordance with the theory of statistical hypothesis testing.

The final results of the simulation studies of the mathematical model and experimental studies of a full-sized marine engine should take the form of a function defining the heat release during fuel combustion, as well as the in-cylinder pressure, in terms of the crankshaft rotation angle.

Simulation studies of appropriately verified mathematical models, which approximately represent the performance of a real object under conditions involving changes to the values of its structural parameters (i.e. simulations of various types of operational failure), make it possible to identify diagnostic symptoms and syndromes [17].

SIMULATION MODEL: A DIGITAL TWIN

Mathematical simulation provides a powerful tool for extracting additional data from diagnostic test results, enabling relatively precise assessment of an engine's technical condition and identification of the potential causes of faults, even when multiple malfunctions are present simultaneously. The most promising application of mathematical simulation is the development of a digital twin for diagnostic purposes, which can accurately replicate the engine's behaviour in terms of diagnostic-relevant aspects [2]. This digital twin should be an integral component of the diagnostic system, whether porTable or stationary. The use of a digital twin may vary based on the types and functionality of the diagnostic systems, and it may be integrated into higher-level digital twins of systems where engines are installed as the power source, such as ships, vehicles, or stationary installations. This approach allows for the computation of transient processes and simulation of intermittent faults, as illustrated in [18]. The greatest benefits can be achieved by combining a digital twin with a learning-capable neural network, as this enables a more efficient and continuous analysis.

A test bench was developed at the Laboratory of the Marne Power Plants and Technical Maintenance at the Odessa National Maritime University (ONMU), based on a Weichai WP4 marine diesel engine powering an electric generator. This test bench was designed for testing new diagnostic methods and systems, particularly those involving digital twin technology. The test bench and its equipment are described in [19], and Fig. 1 shows the primary components.

The test bench is equipped with a set of sensors, including a cylinder gas pressure sensor, fuel pressure sensors at the high-pressure fuel pump outlet and fuel injector inlet, a vibroacoustic sensor, and temperature sensors for the exhaust gases and air within the components of the turbocharging system [20]. The sensor signals are processed by controllers that generate standardised data packets, which are transmitted wirelessly to tablets, as shown in Fig. 2. These tablets run specialised software enabling data processing, analysis, and storage in a database. In addition, the tablets enable streaming of the system's real-time operation to external displays.

This setup allows for real-time diagnostic monitoring of the engine operation, and captures specific diagnostic parameters

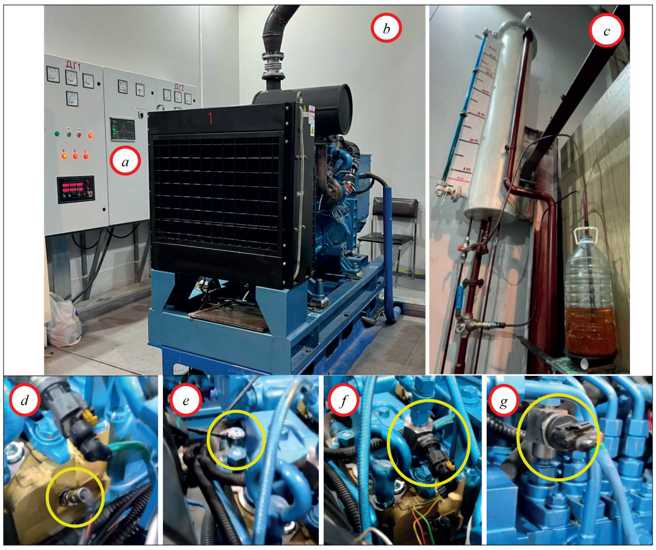

Fig. 1. Photographs of the marine diesel-generator test bench installed in the ONMU laboratory: (a) diagnostic system control panel, (b) general view of the Weichai WP4 marine diesel-generator, (c) fuel consumption measurement piping, (d) cylinder pressure sensor; (e) vibroacoustic sensor, (f), (g) fuel pressure sensors at fuel pump exit and fuel injector entry

associated with cycle irregularities. These parameters and the methodologies for determining them are described in [21].

The online Blitz-PRO service functions as the digital twin, providing automated synthesis of the engine operating processes based on classical thermodynamic equations [22, 23]. A key feature of this simulation service is the incorporation of characteristic maps of turbochargers and superchargers to enable accurate closed-loop modelling of the engine's operating processes under both steady-state and transient conditions, which is especially important for engine operation at various loads and speeds. Specially developed methods allow for simulation of compressor instability, such as surges in the turbocharger's compressor [24].

To model the heat release characteristics, an advanced method developed by Prof. N. F. Razleitsev is used, which accounts for the uneven atomisation of the fuel spray into droplets during injection [2]. In the Razleitsev fuel combustion model, evaporation of the fuel sprays is taken into consideration by applying a modification of the Sreznevsky law for the evaporation of an individual droplet. The fuel evaporation rate is calculated as an integral over all fuel portions injected up to a given moment of time:

$$\frac{d\sigma_{ev}}{d\varphi} = \int_{\varphi inj.start}^{\varphi} \frac{3}{2} \cdot \chi_{\text{wall}} \cdot b_{ev} \cdot \left(1 - \chi_{\text{wall}} \cdot b_{ev} \cdot \frac{\varphi - \varphi_{inj.start}}{6n}\right)^{0.5} \cdot \left[\frac{d\sigma}{d\varphi}\right] d\varphi \quad (1)$$

where:

σ_{ev} – evaporated portion of fuel,
$d\sigma/d\varphi$ – relative injection rate,
b_{ev} – evaporation constant,
χ_{wall} – reduction in the evaporation rate that occurs when fuel interacts with the walls.

The fuel evaporation constant depends on the Sauter diameter of the fuel spray droplets d_{32}, and is calculated as:

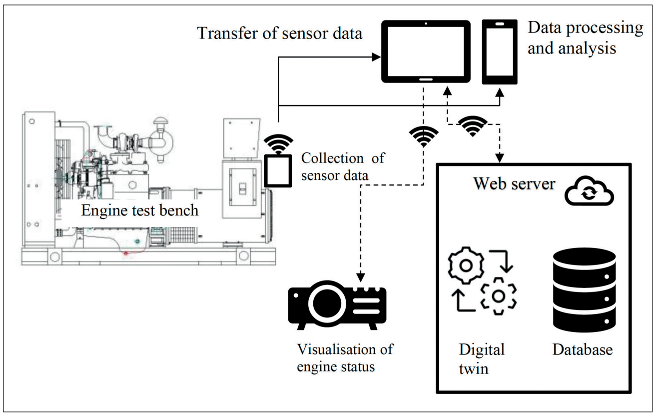

Fig. 2. Diagram of the diagnostic system developed for the test bench

$$b_{ev} = Y \cdot \frac{10^{12}}{d_{32}^2} \cdot \frac{1}{p_c} \quad (2)$$

where:

Y – correction factor,
p_c – end pressure of the compression process,
m_Y – exponent of the evaporation function.

The average Sauter diameter for the fuel droplets is calculated as follows:

$$d_{32} = 10^6 \cdot E_c \cdot d_{inj.holes} \cdot \frac{M^{0.0733}}{(\bar{\rho}\, We)^{0.266}} \quad (3)$$

$$M = \frac{\mu_{fuel}^2}{d_{inj.holes} \cdot \rho_{fuel} \cdot \sigma_{fuel}} \quad (4)$$

$$\bar{\rho} = \frac{\rho_c}{\rho_{fuel}} \quad (5)$$

$$We = \frac{u_{inj}^2 \cdot d_{inj.holes} \cdot \rho_{fuel}}{\sigma_{fuel}} \quad (6)$$

where:

$\mu_{fuel}, \rho_{fuel}, \sigma_{fuel}$ – dynamic viscosity, specific gravity and surface tension of the fuel, respectively,
E_c – an adjusTable coefficient, usually equal to 1.7 for typical nozzles,
$D_{inj.holes}$ – diameter of the nozzle holes,
u_{inj} – injection velocity.

The original approach devised by Razleitsev assumes a constant size of fuel droplets during injection, whereas the modified model accounts for variation based on fuel injection diagrams.

The formation of pollutants during fuel combustion in engine cylinders (specifically nitrogen oxides, carbon monoxide, and soot) is calculated using the methodologies detailed in [25]. For a diesel engine, the main component of greenhouse gases is CO_2, and its amount in the exhaust gases obviously depends on the fuel consumption:

$$g_{CO_2} = g_C \cdot b_b, \frac{g}{kW \cdot h} \quad (7)$$

where:

g_C – carbon mass fraction in engine fuel,
b_b – specific fuel oil consumption for the brake.

Blitz-PRO also provides estimations for the following toxic emission components of the exhaust gases of marine diesel engines: CO, soot, SO_x and NO_x.

The two-zone combustion model is used to predict the gas compositions separately for the fresh charge and burned gas zones. The gas composition for the burned gas zone is calculated using Prof. V. Zvonov's method, in which the burned gases are assumed to form an 18-component mixture of O, O_2, O_3, H, H_2, OH, H_2O, C, CO, CO_2, CH_4, N, N_2, NO, NO_2, NH_3, HNO_3, and HCN.

The NOx concentration at the exhaust gas is calculated based on the Zeldovich mechanism for "thermal" nitric oxide (NO). This chained mechanism includes three equations:

$$N_2 + O \underset{K_{1r}}{\overset{K_{1p}}{\Leftrightarrow}} NO + N \tag{8}$$

$$N + O_2 \underset{K_{2p}}{\overset{K_{2\Pi}}{\Leftrightarrow}} NO + O \tag{9}$$

$$N + OH \underset{K_{3R}}{\overset{K_{3p}}{\Leftrightarrow}} NO + O \tag{10}$$

where:

K_{1p}, K_{1r}, K_{2p}, K_{2r}, K_{3p}, K_{3r} – constants for the direct and reverse chemical reactions, respectively.

The most important formula in terms of the total NO formation kinetics is Eq. (9). The equation for NO kinetics can be expressed as:

$$\frac{d[NO]}{d\tau} = K_{1p}[N_2][O] - K_{1r}[NO][N] + K_{2p}[O_2][N] - K_{2r}[NO][O] + K_{3p}[N][OH] - K_{3r}[NO][H] \tag{11}$$

where the square brackets "[]" express the volumetric concentration of the corresponding matter.

Blitz-PRO currently use the NO formation kinetic equation, which considers only equations (8) and (9) according to Zvonov's approach:

$$\frac{d[NO]}{d\tau} = \frac{2K_{1p}[N_2][O]}{1+\frac{K_{1r}[NO]}{K_{2p}[O_2]}}\left(1 - \frac{[NO]^2}{K_4[O_2][N_2]}\right) \tag{12}$$

$$K_4 = \frac{K_{1p} \cdot K_{2p}}{K_{1r} \cdot K_{2r}} \tag{13}$$

We note that $K_4[O_2][N_2]=[NO]_{eq}$ is the equilibrium concentration of NO.

Conversion of this equation into volumetric fraction units gives:

$$\frac{d[NO]}{d\tau} = \frac{p}{R \cdot T_{burned}} \frac{2K_{1p}[N_2][O]}{1+\frac{K_{1r}[NO]}{K_{2p}[O_2]}} \cdot \left(1 - \left(\frac{[NO]}{[NO]_{eq}}\right)^2\right) \tag{14}$$

where:

p – pressure in the cylinder, bar,
R – gas constant, 8.3144 J/(mole·K),
T_{burned} – temperature of the burned gases.

The Arrhenius law equations are used to calculate the reaction rate constants as follows:

$$K = A \cdot T^B \cdot exp\left(-\frac{E_a}{RT}\right) \tag{15}$$

where:

A, B – empirical coefficients,
E_a – activation energy.

For high-speed engines, the final concentration of CO in exhaust gases is estimated as an equivalent concentration at the end point of combustion. For medium- and low-speed diesel engines, the following kinetic equation is used:

$$\frac{d[CO]}{d\tau} = -K_{1c}[CO][OH] \tag{16}$$

where:

K_{1c} – reaction constant, $7.1 \cdot 10^{12} \cdot \exp(-32200RT)$,
[CO], [OH] – concentrations of CO and OH, respectively.

Soot formation is calculated using Razlejtsev's approach. The instantaneous volumetric soot concentration rate is given by the equation:

$$\frac{d[C]}{d\tau} = \left(\frac{d[C]}{d\tau}\right)_{kin} + \left(\frac{d[C]}{d\tau}\right)_{pol} - \left(\frac{d[C]}{d\tau}\right)_{burn} - \left(\frac{d[C]}{d\tau}\right)_{vol} \tag{17}$$

where:

$\left(\frac{d[C]}{d\tau}\right)_{kin}$ – kinetic formation rate of soot (in the flame),

$\left(\frac{d[C]}{d\tau}\right)_{pol}$ – core polymerisation rate of fuel droplets,

$\left(\frac{d[CO]}{d\tau}\right)_{burn}$ – burning rate of the soot particles,

$\left(\frac{d[C]}{d\tau}\right)_{vol}$ – change in the soot concentration rate due to changes in cylinder volume.

$$\left(\frac{d[C]}{d\tau}\right)_{kin} = B_{1soot} \cdot \frac{q_{fuel}}{V} \cdot \frac{dx}{dt} \tag{18}$$

$$\left(\frac{d[C]}{d\tau}\right)'_{pol} = B'_{2soot} \cdot \delta_d \cdot \frac{q_{fuel}}{V} \cdot \frac{1-exp\left(-\left(\frac{\sqrt{K_{ev} \cdot (\tau - \tau_{inj.start})}}{d_{32}^{inst}}\right)^{n_{disp}}\right)}{\tau_{inj}} \tag{19}$$

$$\left(\frac{d[C]}{d\tau}\right)''_{pol} = B''_{2soot} \cdot \delta_d \cdot (1 - x_{inj.end}) \cdot \frac{n_{disp} \cdot q_{fuel}}{2 \cdot V \cdot (\tau - \tau_{inj.end})} \left(\frac{\sqrt{K_{ev} \cdot (\tau - \tau_{inj.start})}}{d_{32}^{inst}}\right)^{n_{disp}} \frac{1-exp\left(-\left(\frac{\sqrt{K_{ev} \cdot (\tau - \tau_{inj.start})}}{d_{32}^{inst}}\right)^{n_{disp}}\right)}{\tau_{inj}} \tag{20}$$

$$\left(\frac{d[C]}{d\tau}\right)_{burn} = B_{3soot} \cdot k_{O_2} \cdot \sqrt{n} \cdot p \cdot [C] \tag{21}$$

$$\left(\frac{d[C]}{d\tau}\right)_{vol} = B_{4soot} \cdot \frac{6n}{V} \cdot \frac{dV}{d\phi} \tag{22}$$

where:

B_{1soot}, B'_{2soot}, B''_{2soot}, B_{3soot}, B_{4soot} – empirical coefficients,
δ_d – core size of droplets,
d_{32}^{inst} – instantaneous Sauter diameter of the injected fuel,
K_{ev} – evaporation constant,
$\tau_{inj.start}$, $\tau_{inj.end}$ – times of the start and end of injection, respectively,
$x_{inj.end}$ – burned fuel fraction at the end of injection,
n_{disp} – distibution constant (used to consider fuel injection uniformity),
[C] – volumetric soot concentration.

The use of a digital twin enables extensive analysis of the engine performance parameters based on limited sensor data.

Fig. 3 presents a comparison between the indicator diagrams obtained experimentally from the operation of the engine and the output of the digital twin simulation. In this example, the digital twin received the following input data:

– crankshaft rotation speed,
– peak combustion pressure,
– indicator cycle power,
– start of combustion timing.

In the automated mode, the digital twin identifies the optimal fuel injection timing and injection duration based on the received data, and then transmits the calculation results for comparison with the experimental data. Fig. 3 shows a high degree of correspondence between the calculated results and the data experimentally acquired from the cylinder gas pressure sensor. It is notable, however, that while the sensor records distinct non-stationary phenomena during combustion, as explained by pressure wave propagation and wall reflections within the combustion chamber, the calculated curve represents the averaged cylinder pressure, omitting these combustion-specific details.

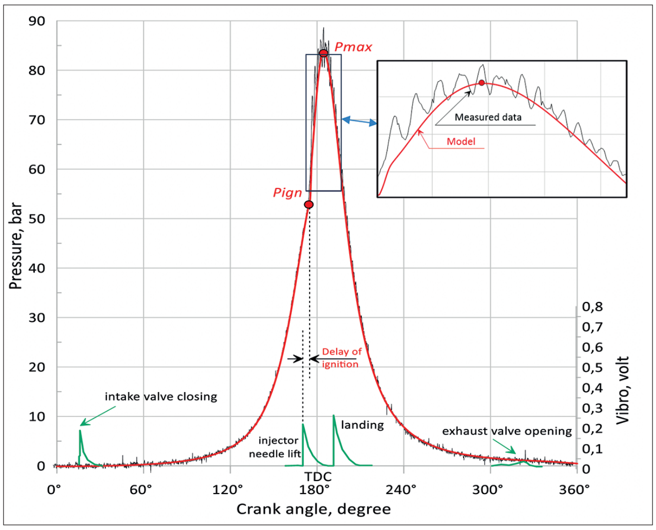

Fig. 3. Comparison of measured cylinder gas pressure data with results from digital twin model

RESULTS AND DISCUSSION

The digital twin can also be used to assess the impact of leakages in precision pairs of injection pumps, as well as the effects of fuel properties on the operational process parameters of the engine, including deviations caused by standard fuels with properties outside specification limits (ISO 8217 Fuel Standard). Such insights are essential for diagnosing deviations in engine performance that may stem from both mechanical issues and fuel characteristics [26].

As part of our simulation studies of the engine operation process using the Blitz-PRO computer program, the following states of the engine fuel fed system were considered:

- FSR (reference state): Engine fed with marine gas oil (MGO) fuel, with standard physicochemical properties;
- FS1: Engine fed with marine diesel oil (MDO) fuel, with standard physicochemical properties;
- FS2: Engine fed with MDO fuel, with non-standard physicochemical properties, except that the value of the fuel kinematic viscosity was increased from 2.37 to 5.16 mm²/s. We note that the standard viscosity value for MDO, determined at 40°C, should be within the range 2.00–4.50 mm²/s. This is a key parameter for the proper functioning of the injection system, as it affects the quality of fuel atomisation and the lubrication of precision pairs of injection pumps and injectors;
- FS3: Engine fed with standard MGO fuel, with simultaneous wear of precision pairs of the injection pump.

Table 1 summarises the steady-state simulation results for a Weichai WP4 engine operating at a crankshaft rotational speed of 1500 rpm, with a set fuel dose of 25.6 mg per cycle and an injection advance angle of 8.5 °CA bTDC. Fig. 4 shows the relational model of the engine working process taking into account the forcings from the considered states of the fuel-fed system (FS).

Tab. 1. Results of operating process simulations of a Weichai WP4 diesel engine under different states of the fuel-fed system (crankshaft rotational speed 1500 rpm, fuel injection (dose) 25.6 mg per cycle)

No	Diagnostic parameter *DP*	FS_R	FS_1	FS_2	FS_3
1	Brake power *BP*, kW	14.51	14.318	14.203	14.26
2	Air excess ratio λ, -	3.916	3.886	3.895	3.937
3	Specific fuel consumption *SFC*, g/(kW·h)	317.7	321.8	324.4	323.09
4	Indicated power *IP*, kW	25.328	25.068	24.887	25.266
5	Maximum in-cylinder pressure p_{cmax}, bar	86.78	84.02	81.79	77.62
6	Maximum in-cylinder temperature t_{cmax}, C	1204.5	1165.6	1133.5	1107.8
7	Maximum temperature in the burned gases zone t_{czmax}, °C	2921.9	2844.5	2833.8	2855.8
8	Self-ignition (firing) pressure p_{csi}, bar	53.74	55.65	55.76	55.15
9	Self-ignition (firing) temperature t_{csi}, °C	945.6	948.9	949.2	948.3
10	Temperature before turbine t_{TC}, °C	255.3	257.4	262.1	268.3
11	Maximum pressure rise rate $(dp_c/d\alpha)_{max}$, bar /°CA.	5.73	10.62	8.87	3.39
12	Injection advance α_{ina}, °CA before TDC	8.5	8.5	8.5	6.5
13	Duration of injection α_{ind}, °CA.	6.8	6.7	6.7	10
14	Average fuel droplets size by Sauter d_{fd}, mcm	20.38	20.60	23.07	24.99
15	Ignition delay α_{igd}, °CA.	2.48	4.09	4.09	2.42
16	Average injection pressure p_{inav}, MPa	28.62	28.75	28.69	16.7
17	Maximum injection pressure p_{inmax}, MPa	50.86	51.27	51.21	26.9
18	CO_2 specific emissions e_{CO_2}, g/(kW·h)	1004.7	1022.2	1030.5	1021.9
19	NO_x specific emissions e_{NO_x}, g/(kW·h)	8.96	8.58	8.42	8.58
20	Soot concentration at exhaust opening referred to normal conditions, in *HSU*, %	0.038	0.066	0.157	0.236

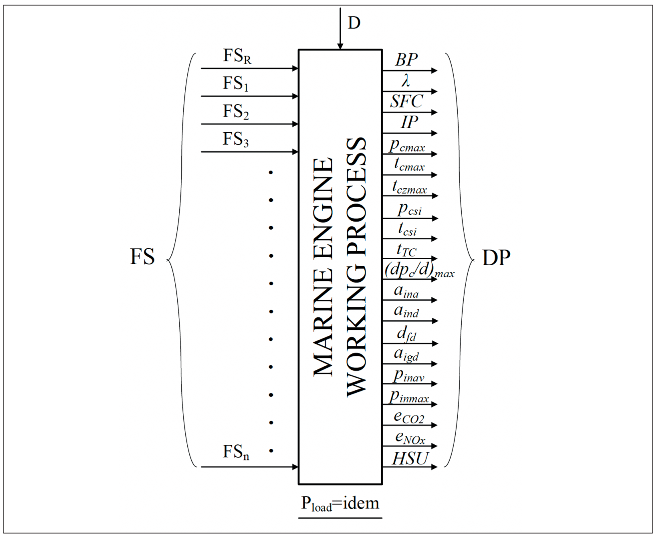

Fig. 4. Relational model of the working process of a marine engine for diagnostic purposes: FS – states of the engine fuel-fed system (forcings), DP – diagnostic parameters (responses), D – disturbances

The numerical data in Table 1 show that the fuel type markedly affects the peak combustion pressure and combustion intensity. Due to the lower cetane number for MDO relative to MGO, the ignition delay extends from 2.48 to 4.09°CA, thereby increasing the proportion of fuel undergoing kinetic combustion, as depicted in Fig. 5. Differences in the lower heating value and evaporation rate reduce the engine power for a given fuel supply, and raise the brake specific fuel consumption from 317.7 g/(kW·h) for MGO to 321.8 and 324.4 g/(kW·h) for conditional and non-conditional MDO, respectively.

These combustion characteristics influence the formation of pollutants within the cylinder. Due to the higher calorific value and faster burn rate of MGO, temperature in burned gases zone elevates, which promotes the conditions necessary for NOx formation, with emission rates reaching 8.96 g/(kW·h) versus 8.58 g/(kW·h) for MDO. Conversely, more efficient combustion lowers the exhaust opacity. Fig. 5 illustrates the dynamics of NO and soot formation in the engine cylinder, while Fig. 6 presents a comparison of the injection-evaporation-combustion diagrams for MGO and MDO, revealing that the ignition delay and evaporation rate are critical factors which make up the effect on the fuel combustion rate diagrams.

For comparison, additional calculations were performed for the engine's operating processes using MGO fuel, with simulations of the wear on the plunger pair of the high-pressure fuel pump. Wear of the plunger pair results in increased fuel leakage, which in turn reduces the injection advance angle from 8.5 to 6.5°CA before TDC and extends the injection duration from 6.7 to 10°CA. The calculated data for this scenario are also presented in Table 1 and Fig. 5.

The interrelationships between the set of states of the fuel-fed system considered here, i.e. $FS_i = \{FS1, FS2, FS3\}$, and the selected set of diagnostic parameters $DP_j = \{BP, \lambda, SFC, \mathrm{IP}, p_{cmax}, t_{cmax}, t_{czmax}, p_{csi}, t_{csi}, t_{TC}, (dp_c/d\alpha)_{max}, \alpha_{ina}, \alpha_{ind}, d_{fd}, \alpha_{igd}, p_{inav}, p_{inmax}, e_{CO2}, e_{NOx}, HSU\}$ identifying these states are usually presented by means of a binary diagnostic matrix, as shown in Table 2. If a diagnostic parameter responded to a change in the fuel-fed

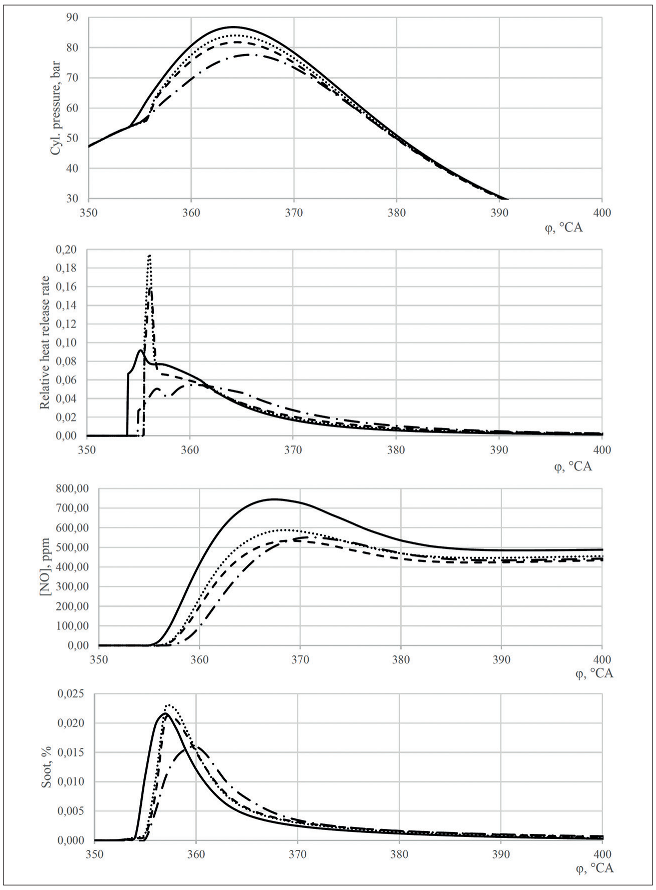

Fig. 5. Simulation results for operation of a Weichai WP4 diesel engine with different fuel properties (as shown in Table 1): ---------- MGO, ·········· MDO, - - - - - - MDO (non conditional), - · - · - MGO (low injection pressure)

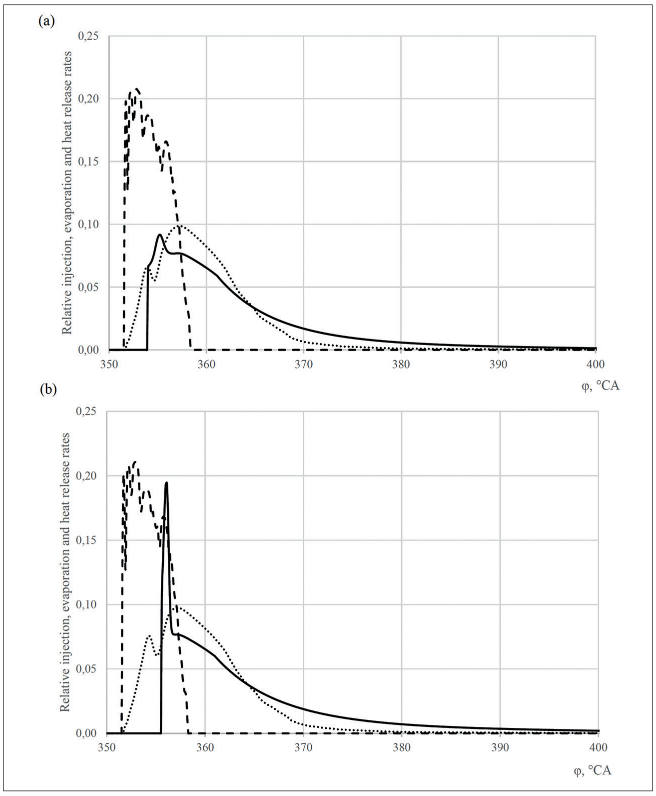

Fig. 6. Comparison of fuel injection, evaporation and combustion rates for (a) MGO and (b) MDO: ---------- fuel combustion rate, ·········· fuel evaporation rate, - - - - - - fuel injection rate

Tab. 2. Diagnostic matrix for the Weichai WP4 diesel engine for the considered states of the fuel-fed system

FS_i/DP_j	BP	λ	SFC	IP	p_{cmax}	t_{cmax}	t_{czmax}	p_{csi}	t_{csi}	t_{TC}
FS_1	0	0	0	0	0	0	0	0	0	0
FS_2	0	0	0	0	1/↓	1/↓	0	0	0	0
FS_3	0	0	0	0	1/↓	1/↓	0	0	0	1/↑

FS_i/DP_j	$(dp_c/d\alpha)_{max}$	α_{ina}	α_{ind}	d_{id}	α_{igd}	p_{inav}	p_{inmax}	e_{CO2}	e_{NOx}	HSU
FS_1	1/↑	0	0	0	1/↑	0	0	0	0	1/↑
FS_2	1/↑	0	0	1/↑	1/↑	0	0	0	1/↓	1/↑
FS_3	1/↓	1/↓	1/↑	1/↑	0	1/↓	1/↓	0	0	1/↑

system state by exceeding the tolerance limits by 5% (becomes a symptom of the change), then a value of one was inserted in the diagnostic matrix cell at the intersection of the i-th row and the j-th column; if the parameter did not respond to a change in state, a value of zero was inserted.

An analysis of the numerical data contained in the matrix indicates that if the diagnostic syndrome result $\{Sd_{FS1}\}=\{0,0,0,0,0,0,0,0,0,0,1,0,0,0,1,0,0,0,0,1\}$ appears during the engine testing process, this indicates that the engine is likely to have been switched to standard MDO fuel. The result $Sd_{FS2}\}=\{0,0,0,0,1,1,0,0,0,0,1,0,0,1,1,0,0,0,1,1\}$ immediately indicates a significant decrease in the viscosity of standard MDO fuel, whereas the result $\{Sd_{FS3}\}=\{0,0,0,0,1,1,0,0,0,1,1,1,1,0,1,1,0,0,1\}$ means that the injection pump has lost its internal tightness, probably due to wear of its precision pair.

In subsequent stages of diagnostic investigations, the set of diagnostic parameters should be minimised using the following elimination criteria:

- The amount of diagnostic information provided about the states of the fuel-fed system, evaluated based on an informative entropy function [27],
- The capabilities of stationary and porTable measurement systems to observe diagnostic parameters selected through simulation studies,
- The controllability of the engine type under test (e.g. whether it is equipped with indicator cocks).

Another example of the application of a digital twin involves the analysis of valve timing compliance with factory specifications and a study of their influence on the engine's operating parameters. During operation of the engine, valve timing may shift for various reasons, including camshaft wear, as described in the first part of this study [28]. In low-speed two-stroke engines, changes in the opening and closing timings of the exhaust valve may occur due to wear of the hydraulic valve actuation system, which requires continuous monitoring at engine operation [22]. Another likely cause is camshaft misalignment during reassembly of the engine after repair.

As shown in Fig. 7, modern diagnostic systems for marine engines equipped with vibration sensors are capable of directly detecting the moment of valve closure and, in some cases, valve opening. For example, the report generated by the DEPAS 5.0W system in Fig. 7 includes the automatically identified intake and exhaust valve closure phases (φ_{IVC}, φ_{EVC}), as well as the intake valve opening phase (φ_{IVO}). The detected phases correspond to the rated specifications. However, during engine reassembly, there is a risk of incorrect camshaft installation relative to the crankshaft. Fig. 8 shows the gear train arrangement of the Weichai WP4 engine; it can be seen that the crankshaft driving gear has 34

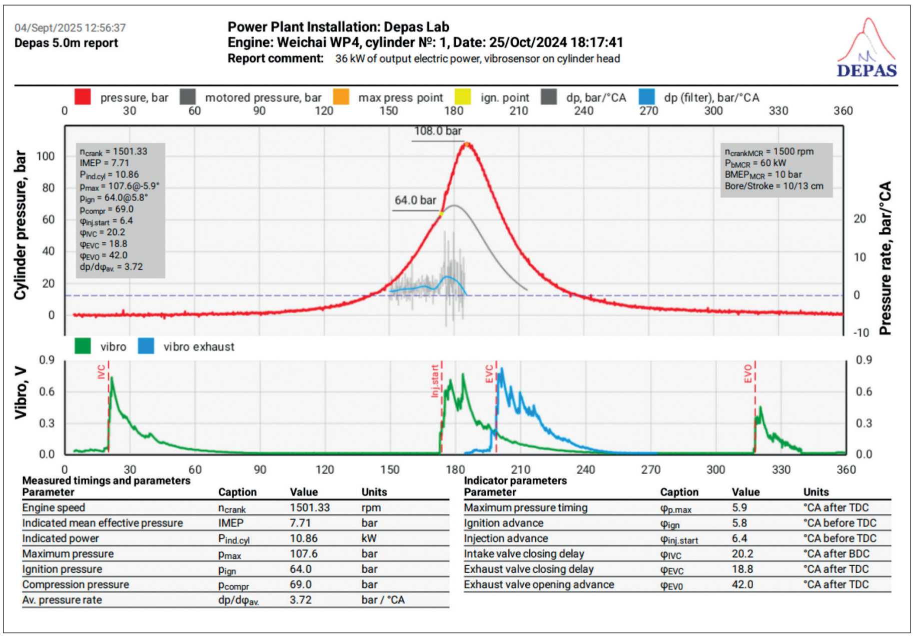

Fig. 7. Report sheet automatically generated by DEPAS 5.0W for the Weichai WP4 test engine

teeth, meaning that installation errors are possible in increments of approximately 10.6° of crankshaft rotation for each missed tooth of the gear.

Using a digital twin, it can be demonstrated that under a load of 36 kW at 1500 rpm (about 60% of the rated power), a camshaft installation error of one or two teeth in the direction of either advanced or delayed valve timing does not prevent the engine from running, meaning that detection of this error without measuring the valve timing directly may be challenging. Nevertheless, as shown in Fig. 9, the main operating parameters of the engine under these operating conditions strongly depend on the camshaft positioning. Incorrect camshaft installation leads to increased fuel consumption, higher exhaust gas temperatures before the turbocharger turbine, and noticeable deviations in peak combustion pressure and ignition pressure.

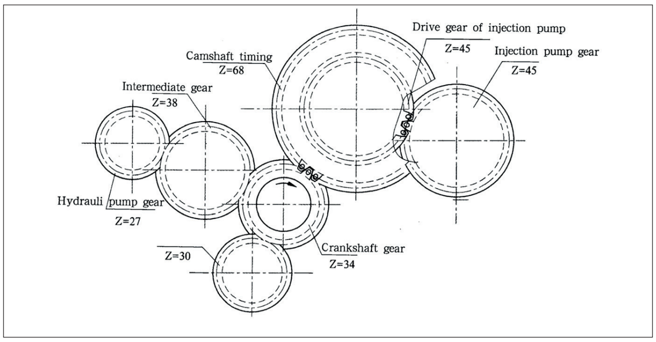

Fig. 8. Diagram showing the gears of the Weichai WP4

Fig. 10 presents pumping-loop *p-V* diagrams and indicator *p-φ* diagrams for the combustion phase for normal camshaft installation, as well as for a camshaft timing shifted by 20° of crankshaft rotation in both the advance and delay directions. A clear increase in pumping-loop power P_{pump} under the shifted timing can be observed, with the numerical values presented in Fig. 9. Thus, a camshaft installation error of two gear teeth may result in an increase in fuel consumption of up to 6% and an exhaust gas temperature rise Δt_t of up to 90°C before the turbine, which adversely affects both the engine efficiency and service life. The diagnostics matrix could also be applied in this case, although direct measurements of the valve timing are preferred if possible.

At higher engine loads, a camshaft installation error becomes evident, since the engine is unable to achieve the rated power without exceeding the exhaust gas temperatures limits.

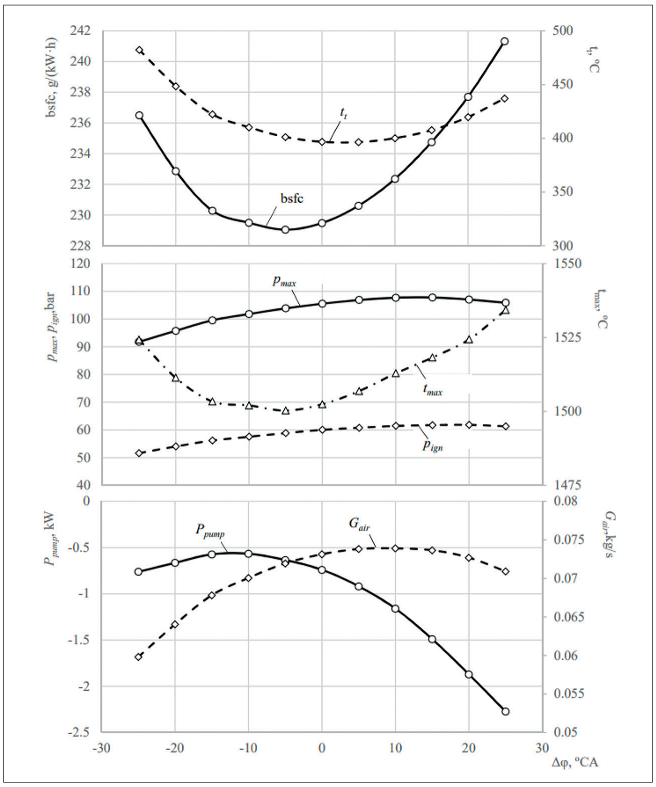

Fig. 9. Effect of camshaft timing on engine performance at a constant load of 36 kW/1500 rpm

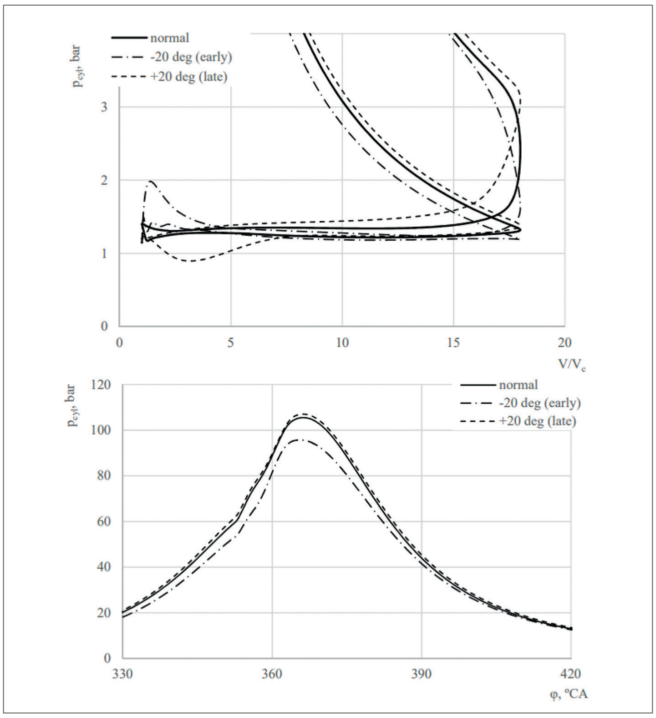

Fig. 10. Effect of camshaft timing on cylinder pressure build-up at a constant load of 36 kW/1500 rpm

CONCLUSION

The results of numerical simulations of the engine working process confirm that the digital twin allows for effective separation of the impact of specific or combined fuel parameter variations on engine performance. This means that these effects can be distinguished from those due to wear in fuel system components as well as deviations of valve timings from the specified values. Our results show that fuel quality and injection system wear strongly influence the ignition delay, peak pressure, combustion rate, and formation of pollutants, with measurable impacts on brake-specific fuel consumption and emission levels. Errors in camshaft installation of one or two gear teeth do not immediately disable the operation of the engine, but lead to increased fuel consumption, higher exhaust gas temperatures, and reduced efficiency, thus highlighting the diagnostic importance of valve timing control.

Integration of the Blitz-PRO simulation service into the diagnostic system enabled accurate replication of transient processes and prediction of irregular operating states, including fuel spray evaporation, turbocharger instabilities, and the formation of emissions. The resulting digital twin, when combined with real-time data acquisition, provided a comprehensive diagnostic framework that was capable of addressing both mechanical wear and fuel-related factors.

This study confirms that digital twin technology, particularly when complemented by advanced combustion and emission models, serves as a powerful tool for real-time diagnostics and condition monitoring of marine diesel engines. Its application not only enhances the accuracy of fault detection but also supports compliance with operational efficiency and environmental protection requirements, thereby extending engine service life and ensuring more reliable operation of diesel power systems.

REFERENCES

1. Nath K, Kumar V, Smith DJ, Karniadakis GE. A digital twin for diesel engines: Operator-infused PINNs with transfer learning for engine health monitoring. Cornell University, December 17, 2024. https://doi.org/10.48550/arXiv.2412.11967.

2. Minchev D, Varbanets R, Shumylo O, Zalozh V, Aleksandrovska N, Bratchenko P, Truong TH. Digital twin test-bench performance for marine diesel engine applications. Polish Maritime Research 2023, Vol. 30, no. 4, pp. 81-91. https://doi.org/10.2478/pomr-2023-0061.

3. Hu D, Wang H, Yang C, Wang B, Duan B, Wang Y, Li H. Construction of digital twin model of engine in-cylinder combustion based on data-driven. Energy 2024, Vol. 293, p. 130543. https://doi.org/10.1016/j.energy.2024.130543.

4. Sagin SV, Solodovnikov VG. Estimation of operational properties of lubricant coolant liquids by optical methods. International Journal of Applied Engineering Research 2017, Vol. 12, no. 19, pp. 8380-8391.

5. Sagin SV, Karianskyi S, Sagin SS, Volkov O, Zablotskyi Y, Fomin O, Píštěk V, Kučera P. Ensuring the safety of maritime transportation of drilling fluids by platform supply-class vessel. Applied Ocean Research 2023, Vol. 140, p. 103745. https://doi.org/10.1016/j.apor.2023.103745.

6. Kafar I, Merkisz J, Piaseczny L. Fuel spray model in a medium speed marine engine—A simulation. Combustion Engines 2006, Vol. 126, no. 3, pp. 63-76. https://doi.org/10.19206/ce-117345.

7. Hahn T. Ignition study in rapid compression machine. Thesis, Massachusetts Institute of Technology, 2009. http://hdl.handle.net/1721.1/46641.

8. Wadkar C, Chinnathambi P, Toulson E. Analysis of rapid compression machine facility effects on the auto-ignition of ethanol. Fuel 2020, Vol. 264, 116546. https://doi.org/10.1016/j.fuel.2019.116546.

9. Bilousov I, Bulgakov M, Savchuk V. Modern marine internal combustion engines: A technical and historical overview. Springer Series on Naval Architecture, Marine Engineering, Shipbuilding and Shipping, 2020. https://doi.org/10.1007/978-3-030-49749-1.

10. Ghojel JI. Review of the development and applications of the Wiebe function: A tribute to the contribution of Ivan Wiebe to engine research. International Journal of Engine Research 2010, Vol. 11, p. 297-312. https://doi.org/10.1243/14680874JER06510.

11. Basurko OC, Uriondo Z. Condition-based maintenance for medium speed diesel engines used in vessels in operation. Applied Thermal Engineering 2015, Vol. 80, p. 404-412. https://doi.org/10.1016/j.applthermaleng.2015.01.075.

12. Korczewski Z. Test method for determining the chemical emissions of a marine diesel engine exhaust in operation. Polish Maritime Research 2021, Vol. 28, no. 3(111), pp. 76-87. https://doi.org/10.2478/pomr-2021-0035.

13. Melnyk O, Bychkovsky Y, Onishchenko O, Onyshchenko S, Volianska Y. Development of the method of shipboard operations risk assessment quality evaluation based on experts review. Studies in Systems, Decision and Control 2023, Vol. 481, pp. 695-710. https://doi.org/10.1007/978-3-031-35088-7_40

14. Gutenbaum J. Mathematical modeling of systems. Systems Research Institute of the Polish Academy of Sciences 1992.

15. Cannon RH. Dynamics of physical systems. New York, Dover Publications; 2003.

16. Tamhane AC. Statistical analysis of designed experiments: Theory and applications. Wiley Series in Probability and Statistics; 2009.

17. Tsitsilonis KM, Theotokatos G, Patil C, Coraddu A. Health assessment framework of marine engines enabled by digital twins. International Journal of Engine Research 2023, Vol. 24, no. 7, pp. 3264-3281. https://doi.org/10.1177/14680874221146835.

18. Varbanets R, Shumylo O, Marchenko A, Minchev D, Kyrnats V, Zalozh V, Aleksandrovska N, Brusnyk R, Volovyk K. Concept of vibroacoustic diagnostics of the fuel injection and electronic cylinder lubrication systems of marine diesel engines. Polish Maritime Research 2022, Vol. 29, no. 4, pp. 88-96. https://doi.org/10.2478/pomr-2022-0046.

19. Neumann S, Varbanets R, Minchev D, Malchevsky V, Vitalii Zalozh V. Vibrodiagnostics of marine diesel engines in IMES GmbH systems. Ships and Offshore Structures 2023, Vol. 18, no. 11, pp. 1535-1546. https://doi.org/10.1080/17445302.2022.2128558.

20. Varbanets R, Fomin O, Píštěk V, Klymenko V, Minchev D, Khrulev A, Zalozh V, Kučera P. Acoustic method for estimation of marine low-speed engine turbocharger parameters. Journal of Marine Science and Engineering 2021, Vol. 9(3), no. 321, pp. 1-13. https://doi.org/10.3390/jmse9030321.

21. Varbanets R, Minchev D, Kucherenko Y, Zalozh V, Kyrylash O, Tarasenko T. Methods of real-time parametric diagnostics for marine diesel engines. Polish Maritime Research 2024, Vol. 31, no. 3, pp. 71-84. https://doi.org/10.2478/pomr-2024-0037.

22. Minchev D, Varbanets R, Aleksandrovskaya N, Pisintsaly L. Marine diesel engines operating cycle simulation for diagnostics issues. Acta Polytechnica 2021, Vol. 3, no. 61, pp. 428-440. https://doi.org/10.14311/AP.2021.61.0435.

23. Blitz-PRO by D S Minchev. User's manual. Retrieved from http://blitzpro.zeddmalam.com/ extra/Tutorial/Help.pdf.

24. Minchev D, Gogorenko OA, Varbanets RA, Moshentsev YL, Píštěk V, Kučera P, Shumylo OM, Kyrnats VI. Prediction of centrifugal compressor instabilities for internal combustion engines operating cycle simulation. Proceedings of the Institution of Mechanical Engineers, Part D: Journal of Automobile Engineering 2023, Vol. 237, nos. (2-3), pp. 572-584. https://doi.org/10.1177/09544070221075419.

25. Varbanets R, Minchev D, Savelieva I, Rodionov A, Mazur T, Psariuk S, Bondarenko V. Advanced marine diesel engines diagnostics for IMO decarbonization compliance. AIP Conf. Proc. 16th February 2024, vol 3104, no. 1, p. 020004. https://doi.org/10.1063/5.0198828.

26. Melnyk O, Onishchenko O, Onyshchenko, S. Renewable energy concept development and application in shipping industry. Lex Portus 2023, Vol. 9, no. 6, pp. 15-24. https://doi.org/10.26886/2524-101X.9.6.2023.2.

27. Korczewski Z. An entropy function application within the selection process of diagnostic parameters of marine diesel and gas turbine engines. Polish Maritime Research 2010, Vol. 2(65), no. 17, pp. 29-35. https://doi.org/10.2478/v10012-010-0015-2.

28. Korczewski Z, Rudnicki J, Varbanets R, Minchev D. Multi-symptom diagnostic investigation of the working process of a marine diesel engine: Case study. Part 1: Measurement Diagnostics. Polish Maritime Research 2025, Vol. 32, no. 2, pp. 50-61. https://doi.org/10.2478/pomr-2025-0020.

29. ISO 8217:2024. Products from petroleum, synthetic and renewable sources - Fuels (class F) - Specifications of marine fuels. Standard by International Organization for Standardization , 06/01/2024.